Journal of the Mechanics and Physics of Solids 59 (2011) 829–840

Contents lists available at ScienceDirect

Journal of the Mechanics and Physics of Solids

journal homepage: www.elsevier.com/locate/jmps?

Toughness amplification in natural composites

Francois Barthelat *, Reza Rabiei

Department of Mechanical Engineering, McGill University, 817 Sherbrooke Street West, Montreal, Quebec, Canada H3A 2K6

ARTICLE INFO

Article history:
Received 11 May 2010
Received in revised form
1 September 2010
Accepted 2 January 2011
Available online 5 January 2011

Keywords:
Nacre
Bone
Biological composites
Fracture toughness
Micromechanics

ABSTRACT

Natural structural materials such as bone and seashells are made of relatively weak building blocks, yet they exhibit remarkable combinations of stiffness, strength and toughness. This performance can be largely explained by their "staggered microstructure": stiff inclusions of high aspect ratio are laid parallel to each other with some overlap, and bonded by a softer matrix. While stiffness and strength are now well understood for staggered composites, the mechanisms involved in fracture are still largely unknown. This is a significant lack since the amplification of toughness with respect to their components is by far the most impressive feature in natural staggered composites such as nacre or bone. Here a model capturing the salient mechanisms involved in the cracking of a staggered structure is presented. We show that the pullout of inclusions and large process zones lead to tremendous toughness by far exceeding that of individual components. The model also suggests that a material like nacre cannot reach steady state cracking, with the implication that the toughness increases indefinitely with crack advance. These findings agree well with existing fracture data, and for the first time relate microstructural parameters with overall toughness. These insights will prove useful in the design of biomimetic materials, and provide clues on how bone fractures at the nano and microscales.

1. Introduction

Structural biological materials are increasingly attracting the attention of researchers and engineers for their remarkable performances (Wegst and Ashby, 2004; Barthelat, 2007; Ortiz and Boyce, 2008), and their structures and mechanics are therefore at the focus of intense research. Recent advances in experimental and modeling techniques have enabled significant progress in this area. For example in medicine, a better understanding of how bone deforms and fractures will improve the way drugs are targeted to treat diseases such as osteoporosis. In biomimetics, the structures and mechanics of hard biological materials such as bone and nacre are now inspiring novel bio-inspired materials with remarkable properties (Barthelat, 2007, 2010; Ortiz and Boyce, 2008; Munch et al., 2008).

Natural materials use a large variety of structures, mechanisms and ingenious designs to achieve high mechanical performance. Beyond this apparent diversity, examination at smaller length scales however reveals common structural patterns or "universal motives" (Buehler and Yung, 2009) found across biological materials. An excellent case of universal motives is the staggered structure, where stiff inclusions of high aspect ratio (long molecules, fibers or platelets) are embedded in a compliant and ductile organic matrix with some overlap, to form a staggered structure (Jackson et al., 1988; Jager and Fratzl, 2000; Kotha et al., 2001; Gao, 2006; Barthelat et al., 2007). A well known example of such structure is nacre from mollusk shells, where calcium carbonate tablets form a three dimensional staggered brick wall-like structure with softer protein and polysaccharide

* Corresponding author. Tel.: +1 514 398 6318; fax: +1 514 398 7365.
E-mail address: francois.barthelat@mcgill.ca (F. Barthelat).

0022-5096/$ - see front matter © 2011 Elsevier Ltd. All rights reserved.
doi:10.1016/j.jmps.2011.01.001

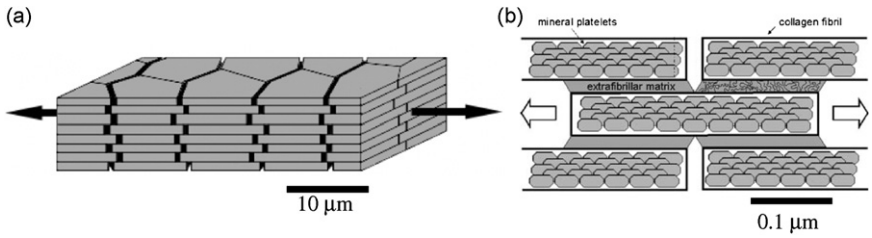

Fig. 1. Example of natural staggered structures: (a) nacre and (b) bone (Gupta et al., 2006).

layers at the interface (Jackson et al., 1988) (Fig. 1a). Under tensile stress the tablets can "slide" on one another, a key mechanism that generates significant deformation and energy dissipation. Another example is collagen fibrils, composed of staggered collagen molecules. In bone the fibrils are mineralized by nanometers size crystals, intercalated with the softer collagen molecules in a staggered fashion (Buehler, 2007) (Fig. 1b). In turn, those fibrils assemble into a staggered structure to form microscopic fibers, the building blocks of bone (Weiner and Wagner, 1998; Gupta et al., 2006). Gliding of the mineralized fibers on one another is an important deformation mechanism in bone (Gupta et al., 2006). Interestingly, bone also has a hierarchical structure where the staggered motif can be found over several length scales (Gao, 2006). In natural staggered composites the stiff inclusions are bonded by softer interfaces capable of maintaining cohesion over large separation distances. The materials found at these interfaces must have high resilience, and it is actually striking that these softer materials have similar structures and mechanics in nacre and bone (Smith et al., 1999; Fantner et al., 2005). Other identified examples of materials with staggered structures are tooth enamel and spider silk (Keten, 2010).

The question of how the staggered microstructure controls structural properties such as modulus, strength and toughness is of high relevance for biomedical and biomimetic applications. The modulus along the long axis of the inclusions can now be predicted with the models developed by Jager and Fratzl (2000) or by Kotha et al. (2001). Both of these models predict that high aspect ratio and high concentration of the inclusions lead to high modulus. To predict strength, shear-lag type models borrowed from composite theories can be used (Jackson et al., 1988). Toughness is more challenging to predict because there are multiple toughening mechanisms at work when a crack propagates in a staggered composite. For example, no less than ten toughening mechanisms were recently proposed for nacre (Mayer, 2005). The few models that captured specific toughening mechanisms in staggered structures include the fracture model by Okumura and de Gennes (2001), who examined the effect of the differential of stiffness between inclusions and interfaces on the toughness, and of the viscoelasticity of the interfaces. Gao (2006) has proposed a fracture model that incorporates bridging by the inclusions and the effect of the hierarchical structure on overall toughness. The possible implications of the small size of the inclusions on their tensile strength were first proposed by Currey (1977), and further elaborated by Gao et al. (2003), although this point remains controversial (Ballarini et al., 2005). Recent experimental work demonstrated the significant contribution of inelastic deformations on the toughness of nacre (Barthelat and Espinosa, 2007; Rabiei et al., 2010). In large regions around cracks the mineral tablets "slide" on one another (Fig. 1a), which dissipates a significant amount of energy that would otherwise be used for crack propagation (Barthelat and Espinosa, 2007). Fracture experiments on various types of nacres strongly suggest that this "process zone" is a prominent toughening mechanism (Rabiei et al., 2010). In bone, a similar sliding mechanism was recently demonstrated using synchrotron X-ray illumination (Gupta et al., 2006). Under tensile stress the mineralized collagen fibrils slide on one another, generating inelastic deformations (Fig. 1b). As opposed to nacre these mechanisms could not be observed directly in the vicinity of cracks, possibly because they involve smaller length scales that are masked by toughening mechanisms operating at larger scales (Ager et al., 2006; Peterlik et al., 2006). There is currently no comprehensive model to capture the mechanics of fracture in staggered composites and in particular, there is no model that properly captures the effect of the inelastic process zone. This is a significant lack, since for these materials it is the toughness which is by far the most spectacular property, and therefore the most attractive property to duplicate in biomimetic materials (Launey and Ritchie, 2009).

The aim of this paper is to provide a condensed approach to predicting relevant structural properties in staggered composites. Existing micromechanics models for modulus and strength are briefly reviewed first and their predictions are compared with available experimental data. Following the same philosophy, a model for the toughness of staggered composites incorporating the micromechanics of crack bridging and process zone is presented. Whenever possible each step of the model is validated with experiments. The results reveal new insights on how staggered structures fracture, and how microstructural parameters control the overall toughness.

2. Basic properties of staggered composites

2.1. Elastic modulus

The basis for modeling the elasticity of staggered structures is the two dimensional representative volume element (RVE) shown in Fig. 2 (Jager and Fratzl, 2000; Kotha et al., 2001). The stiff mineral inclusions (modulus E_m) have a length L

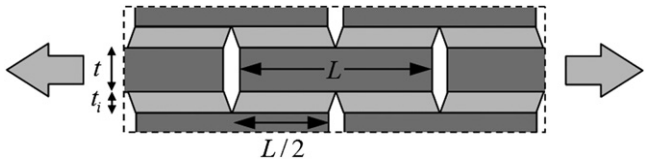

Fig. 2. Periodic representative element of the microstructure of a staggered composite, with applied tensile load shown.

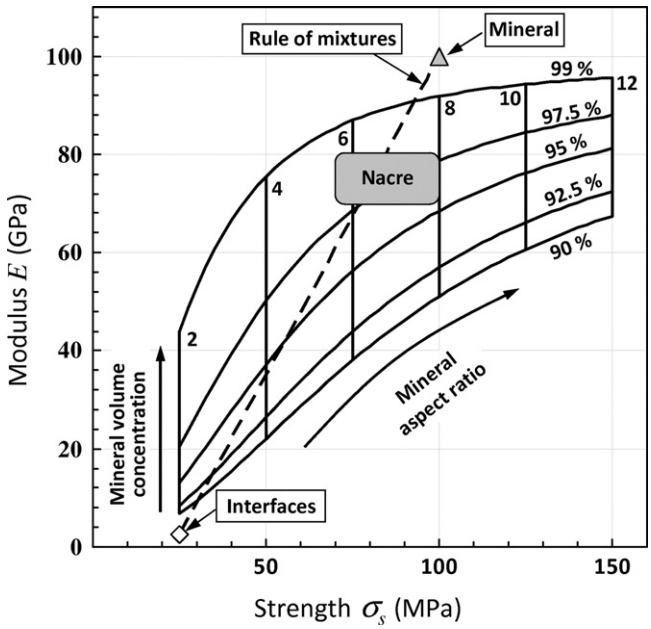

Fig. 3. Comparison of the predictions for modulus and strength with experimental data from red abalone nacre (Wegst and Ashby 2004; Barthelat et al., 2007).

and thickness t, and overlap each other by a length $L/2$ (only half-staggered structures are considered here for simplicity, but actual materials can show large variability in overlap). The softer organic material (shear modulus G_i) forms interfaces of thickness t_i between the inclusions.

Kotha et al. (2001) developed an expression for the modulus E of this composite along the direction of the inclusions. Their result can be written as

$$\frac{1}{E}=\left(1+\frac{t_i}{t}\right)\left(\frac{1}{E_m}+2\frac{t}{L}\frac{t_i\gamma}{G_i}\left(\frac{1+\cosh(\gamma L)}{\sinh(\gamma L)}\right)\right) \tag{1}$$

where

$$\gamma=\sqrt{\frac{G_i}{E_m}\frac{1}{t_i t}} \tag{2}$$

For cases where the interfaces are much softer than the inclusions ($G_i \ll E_m$) $\cosh(\gamma L)\approx 1$ and $\sinh(\gamma L)\approx \gamma L$, so Eq. (1) becomes

$$\frac{1}{E}\approx\left(1+\frac{t_i}{t}\right)\left(\frac{1}{E_m}+4\left(\frac{t}{L}\right)^2\frac{t_i}{t}\frac{1}{G_i}\right) \tag{3}$$

This expression captures the main trends in stiffness of the composite: the modulus increases for thin interfaces (small t_i/t) and large aspect ratios L/t. This model is compared with experimental data in Fig. 3. Note that for large aspect ratio the modulus converges towards the Voigt composite model (with no tension carried by the interfaces, as initially assumed):

$$\lim_{L/t\to\infty}(E)=\frac{t}{t+t_i}E_m \tag{4}$$

Eq. (3) can also be written in terms of the mineral volume density $\phi = t/(t+t_i)$ and of the aspect ratio of the inclusions $\rho = L/t$. With these parameters the Jäger and Fratzl model for bone (Jager and Fratzl, 2000) is recovered:

$$\frac{1}{E} \approx \frac{1}{\phi E_m} + 4\frac{1}{\rho^2}\frac{1-\phi}{\phi^2}\frac{1}{G_i} \tag{5}$$

This form puts more emphasis on the effect of mineral volume density on the modulus.

2.2. Strength

Under tensile load the staggered structure can fail either by fracture of the inclusions or yielding of the softer interfaces. In terms of energy dissipation the latter is much more beneficial, and is the prominent failure mode in nacre (Jackson et al., 1988). The interfaces fail when the shear stress reaches the interface strength τ_S (note that with no hardening the shear stress at failure is uniform along the interface). A simple load transfer model can then be used to predict the tensile strength of the composite. With the assumption that $t_i \ll t$ one obtains

$$\sigma_S = \frac{1}{2}\frac{L}{t}\tau_S \tag{6}$$

In this equation the shear strength of the interface controls the tensile strength of the composite, through a load transfer mechanism whose magnitude depends on the aspect ratio of the inclusions (term (L/t)).

The predictions of these models can be illustrated in a condensed fashion on a material property chart inspired from Wegst and Ashby (2004). Fig. 3 shows the modulus and tensile strength of the mineral in nacre (Wegst and Ashby, 2004), of the interfaces in nacre (Barthelat et al., 2007), and of nacre as a composite (Barthelat et al., 2007). Note that the interfaces in nacre are complex systems consisting of soft layers of proteins and polysaccharides (Sarikaya and Aksay, 1995) together with aragonite nanoasperities (Wang et al., 2001) and bridges (Song and Bai, 2003). All of these elements contribute to the material properties used here (Barthelat et al., 2007). The predictions of the modulus and strength models are also plotted for various mineral aspect ratios and concentrations. The models predict that modulus and strength both increase with aspect ratio and with inclusion volume concentration. The experimental data shown in Fig. 3 for nacre is for red abalone, which has a mineral concentration of about 95% (Currey, 1977), and tablets with aspect ratio of about 12 (Rabiei et al., 2010). The model therefore agrees well with the experiment although the strength is slightly overestimated, which could be due to defects in the material (Barthelat and Espinosa, 2007), to the actual overlap of the tablets in red abalone which is less than half of the tablet length, and also to the fact that a small number of tablets may break prematurely instead of being pulled out.

Finally, note that the model predictions were also plotted in regions exceeding the strength of the mineral. This is consistent with the hypothesis that minerals in nature are stronger than their bulk form because of their small size (Gao et al., 2003).

3. Toughness of staggered composites

3.1. Steady state toughening

The previous two sections discussed existing analytical models for the modulus and tensile strength of staggered composites. In this section a model following the same philosophy is developed to predict toughness. How microstructural parameters control the toughness is of high relevance, since it is the toughness that is the most remarkable property in these materials. The model focuses on a mode I crack running across the long axis of the inclusions, and will make use of the strength and modulus models discussed above. The cohesion of the material is ensured by progressive pullout of the tablets through a mechanism similar to fiber bridging in composites, and with associated cohesive length λ (Fig. 4).

In addition, high stresses ahead of the crack tip generate a frontal zone where the strength of the composite σ_S is reached and where tablets slide on one another. In nacre, this phenomenon is clearly visible because tablet sliding whitens the material (Barthelat and Espinosa, 2007; Rabiei et al., 2010), as a result of an optical effect similar to stress-whitening in polymers. As the crack advances through the frontal zone the material only partially recovers its deformation, forming a wake behind the crack tip. Frontal zone and wake form the process zone of characteristic half-width w (Fig. 4). The next two sections examine how bridging and process zone contribute to the overall toughness of the structure for a crack in steady state condition.

3.1.1. Bridging

Examination of a fracture surface in nacre shows evidence that tablets pullout is the main decohesion mechanism, with rare occurrences of tablet fracture (Jackson et al., 1988). Pullout of inclusions is usually treated as crack bridging, an extrinsic toughening which enhances the intrinsic toughness of the matrix (Lawn, 1993); however, since tablets pullout is the only cohesive mechanism for the staggered structure, its contribution was assimilated to intrinsic toughness. Fig. 5 shows a two dimensional model of the bridging configuration. The pullout mechanism generates a cohesive region of length λ, resulting from the closure forces generated by each tablet involved in pullout.

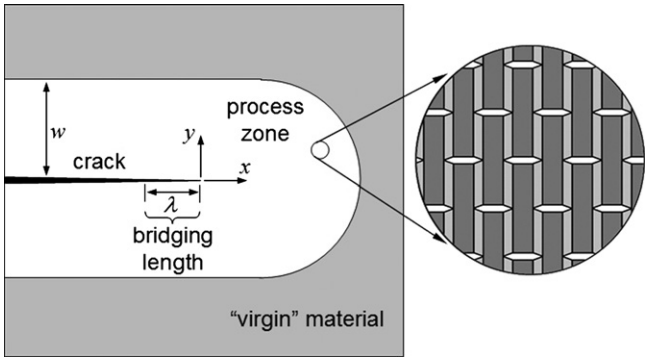

Fig. 4. A crack advancing in a staggered composite. The bridging zone (characteristic length λ) and process zone (half-width w) are shown. In nacre the process zone looks whiter than the surrounding material.

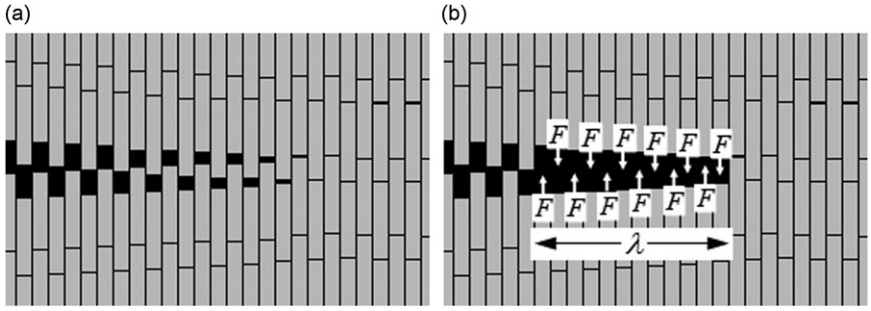

Fig. 5. (a) Pullout of inclusions is the prominent decohesion mechanism in staggered composites and (b) closure forces exerted on the crack faces by the bridging inclusions, over the cohesive length λ.

The pullout of the inclusions is clearly controlled by shearing of the interfaces. Assuming uniform shear strength τ_S for the interfaces, the interface toughness is simply given by

$$J_i = \int_0^{u_{\max}} p(u)du = \tau_S u_{\max} \tag{7}$$

where u_{max} is the sliding distance at which the interface cohesion vanishes. Note that with the realistic values of τ_S= 20–25 MPa (Barthelat et al., 2007) and u_{max}=60–100 nm (Rabiei et al., 2010; Wang et al., 2001) one finds J_i=1.2–2.5 J/m^2, which corresponds to only 1/500 of the overall toughness measured for nacre (Rabiei et al., 2010). Interface toughness, although necessary, is therefore not sufficient to explain the toughness of staggered composites. In order to calculate the bridging contribution, the closure forces carried by the tablets involved in pullout are considered (Fig. 5b). Each of these forces is equal to

$$F = L\tau_S \tag{8}$$

The spacing between the bridging forces is $2t$, and homogenizing this discrete force distribution leads to a continuous closure traction:

$$t(u) = F/2t = \frac{1}{2}\frac{L}{t}\tau_S \tag{9}$$

Note that $t(u)$ can now be seen as a cohesive traction on the crack faces of the composite. The intrinsic toughness of the composite J_0 may now be computed using (Lawn, 1993)

$$J_0 = 2\int_0^{u_{\max}/2} t(u)du \tag{10}$$

which, using (7) and (9), gives

$$J_0 = \frac{1}{2}\frac{L}{t}J_i \tag{11}$$

Eq. (11) shows that bridging amplifies the toughness of the interface by a factor of (½) (L/t). Again, high inclusion aspect ratio leads to higher amplifications. In the experiment, J_0 corresponds to the initial toughness of the material in absence of any extrinsic toughening mechanism.

It is useful to compute the length over which bridging operates in steady state (i.e. cohesive length, Lawn, 1993):

$$\lambda = \frac{\pi}{8}\frac{J_0 E}{\sigma_S^2} \tag{12}$$

Using realistic values for red abalone nacre $L/t \approx 12$ (Rabiei et al., 2010), J_i=1.2–2.5 J/m^2, σ_S=70–100 MPa (Barthelat et al., 2007; Wang et al., 2001), and E=70–80 GPa (Barthelat et al., 2007; Wang et al., 2001), one finds $J_0 \approx$ 7–16 J/m^2 and $\lambda \approx$ 20–100 μm. The actual cohesive length for nacre is difficult to measure because the crack tip cannot be located accurately. Nevertheless, the computed range of values appears reasonable considering experimental observation (Rabiei et al., 2010). The bridging toughness J_0 is about 1/100 that of the toughness of nacre, which suggests that bridging only cannot account for the overall toughness.

3.1.2. Process zone

In materials like nacre and bone the high stresses at the crack tip trigger the sliding of the inclusions on one another over regions several times larger than the inclusion size. In effect, the inclusions separate, a well documented mechanism in nacre (Jackson et al., 1988; Barthelat et al., 2007; Wang et al., 2001) that was also recently demonstrated in bone (Gupta et al., 2006). The sliding and separation of the tablets generate dilation at the microscale, as shown in Fig. 4. This type of mechanism is comparable to rubber toughened polymers, where high stresses ahead of a crack debond rubber precipitates from the matrix, generating voids that subsequently dilate under stress and enabling process zone toughening (Evans et al., 1986). Here the tablets predominantly separate from each other under the action of the longitudinal stress σ_{yy} (the effect of any other stress components on tablet separation is neglected), such that a criterion for tablet sliding is simply $\sigma_{yy}=\sigma_S$. Based on linear elastic asymptotic stress field in plane strain and assuming a Poisson's ratio of 0.2, the half-width of the inelastic zone is given by (Evans et al., 1986)

$$w \approx \frac{1}{4}\frac{JE}{\sigma_S^2} \tag{13}$$

where J and E are the toughness and the modulus of the composite, respectively. With typical values for nacre (σ_S=70–100 MPa (Barthelat et al., 2007; Wang et al., 2001), E=70–80 GPa (Barthelat et al., 2007; Wang et al., 2001) and J=0.5–1 kJ/m^2 (Rabiei et al., 2010)) one finds $w \approx$ 0.8–4 mm, which is in the same order as the actual optical observations (Rabiei et al., 2010; Wang et al., 2001). Assuming a fully developed crack wake in steady state condition, the contribution of the process zone to toughness can now be written (Evans et al., 1986):

$$J = J_0 + \Delta J_P \tag{14}$$

where

$$\Delta J_P = 2\int_0^w U(y)\,dy \tag{15}$$

Here $U(y)$ is the energy dissipated per unit area, given by

$$U(y) = \int_0^{\varepsilon(y)} \sigma\, d\varepsilon \tag{16}$$

The calculation of Eq. (16) requires the knowledge of the distribution of residual strains $\varepsilon(y)$ within the wake. The residual strains are zero at the boundary of the inelastic region (at $y=\pm w$, Fig. 4). At the crack faces, the material deforms by the strain ε_{max}, and recovers some elastic deformation in the wake. For simplicity the modulus is assumed to remain unchanged in the inelastic regime, so that the residual strain at the crack faces is $\varepsilon_{\max}-\sigma_S/E$ (Fig. 6). The simplest distribution that follows these conditions is linear and may be written as

$$\varepsilon(y) = \left(1-\frac{y}{w}\right)\left(\varepsilon_{\max}-\frac{\sigma_S}{E}\right) \tag{17}$$

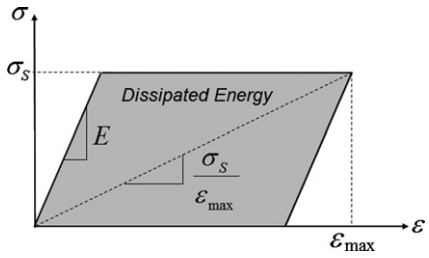

Fig. 6. Stress-strain history of the material near the crack faces.

Experiments have actually revealed that the residual strains in nacre appear to indeed follow a linear distribution (Barthelat and Espinosa, 2007). Combining (15)–(17) leads to the process zone toughening

$$\Delta J_P = \sigma_S\left(\varepsilon_{\max}-\frac{\sigma_S}{E}\right)w \tag{18}$$

Combining (14), (13), and (18) gives

$$J = J_0+\frac{1}{4}\frac{JE}{\sigma_S}\left(\varepsilon_{\max}-\frac{\sigma_S}{E}\right) \tag{19}$$

which can be rewritten as

$$J = \frac{J_0}{1-\alpha} \tag{20}$$

where

$$\alpha = \frac{1}{4}\left(\frac{E\varepsilon_{\max}}{\sigma_S}-1\right) \tag{21}$$

Process zone toughening is therefore multiplicative, as emphasized in Evans et al. (1986). In this equation, the intrinsic toughness J_0 is amplified by a factor $1/(1-\alpha)$. Here the "process zone parameter" α clearly controls the amount of toughness amplification with respect to the intrinsic toughness. α provides a measure of how much energy is dissipated in the wake as the crack advances, or in other words, it is a measure of the efficacy of process zone toughening. Note that α is a function of the ratio between the initial modulus E and the secant modulus at failure $\sigma_S/\varepsilon_{max}$ (Fig. 6). This highlights the influence of the stress–strain curve on process zone toughening. For example for a brittle material $E=\sigma_S/\varepsilon_{max}$, which results in $\alpha=0$ and $J=J_0$ (no process zone). Materials with a high modulus, low strength and high strain at failure result in larger α, which in turn leads to larger process zone and higher toughness. As a result, α should be maximized in order to achieve maximum process zone toughening. At the same time, Eq. (21) only accepts physically meaningful solutions if $\alpha<1$ (i.e. $E<5\sigma_S/\varepsilon_{max}$), an important limitation which is addressed in the next sections.

Combining Eqs. (20), (21), (11), and (7), the toughness can also be expressed in the following form which better highlights the influence of the microstructure:

$$J = \frac{L/t}{2.5-(u_{\max}/L)\,(t/L)\,(E/\tau_S)}J_i \tag{22}$$

This expression is very useful as it reveals the effect of the microstructure on toughness:

(i) Overall the staggered microstructure *amplifies* the toughness of the interfaces.
(ii) The toughness increases with the aspect ratio of the inclusions (term L/t)
(iii) A stiff composite with weak interfaces promotes toughness (term E/τ_S)
(iv) The toughness is greater for large (u_{max}/L) ratios. This suggests that given thin interfaces with a fixed maximum cohesive displacement u_{max}, the size of the microstructure should be minimized in order to maximize overall toughness. This conclusion provides a new explanation for the small length scale of the microstructure in natural composites.

3.2. Non-steady state toughening

As noted above, Eq. (20) accepts a physical solution only if $\alpha<1$. However, stiff materials with low strength and large strains at failure may lead to a process zone parameter greater than 1. Typical properties for red abalone (E=70–80 GPa (Barthelat et al., 2007; Wang et al., 2001), σ_S=70–100 MPa (Barthelat et al., 2007; Wang et al., 2001), and ε_{max}=0.008–0.015 (Barthelat and Espinosa, 2007; Wang et al., 2001; Barthelat and Espinosa, 2007)) lead to α=1.15–4. This means that in materials like nacre steady state cracking cannot be achieved in theory, and that the inelastic wake and the toughness J will keep increasing indefinitely with crack advance (in practice the limitation to this trend is the size of the sample, i.e. the thickness of the shell, Evans et al., 1986). A general model including the non-steady state regime must therefore be developed in order to capture the fracture of a material like nacre.

3.2.1. Bridging

Non-steady regime is first incorporated in the bridging mechanism. With the assumption that the intrinsic cohesion of the material is provided by crack bridging only, the initial toughness is zero. Upon crack advance the cohesive length increases, and the toughness increases accordingly. The closure stress applied over the cohesive length is uniform, and therefore the toughness increases linearly with crack advance a. When the crack length reaches the steady state cohesive length λ (Eq. (12)), the bridging toughness reaches the steady state value J_0. The transient bridging toughness J_B can

therefore be written as

$$\begin{cases} J_B = \frac{a}{\lambda} J_0 & \text{for} \quad 0 \le a \le \lambda \\ J_B = J_0 & \text{for} \quad \lambda < a \end{cases} \tag{23}$$

3.2.2. Process zone

In the non-steady regime, the width of the process zone as defined in Fig. 4 is not constant. In the case of interest here the width of the process zone will increase with crack advance, and the toughness will rise accordingly. This type of problem requires exact knowledge of the deformation behavior of the material, and of the size and the shape of the process zone (McMeeking and Evans, 1982). In the present case only tension along the direction of the tablets is considered as a dilatational and dissipative mechanism. In addition, the shape of the frontal zone is assumed to be circular, which simplifies the calculations while being consistent with experimental observations (Barthelat and Espinosa, 2007; Rabiei et al., 2010). The process zone contribution to the toughness is taken as the amount of energy dissipated in the wake per surface area generated upon crack advance. In order to estimate this energy, a geometrical construction of a widening wake is proposed in Fig. 7. High stresses ahead of the tip generate inelastic deformation in a circular frontal zone of radius w. With the assumption that the stiffness of the material is unaffected by the sliding of the tablets, the frontal zone has no influence on toughness before crack propagation starts (Evans et al., 1986; McMeeking and Evans, 1982). Upon crack advance by a small increment da, fresh material deforms inelastically, generating a frontal zone of larger radius (radius $w+dw$) while regions of the former frontal zone are unloaded, forming a wake. Lines tangent to both circles define an incremental wake region dW (hatched region in Fig. 7).

The energy dU_P dissipated in the incremental wake is given by

$$dU_P = \iint_{dW} U(x,y)\,dx\,dy = \iint_{dW} \sigma_S\left(\varepsilon_{\max} - \frac{\sigma_S}{E}\right)\left(1 - \frac{y}{w(x)}\right) dx\,dy \tag{24}$$

This integral was calculated analytically to yield

$$dU_P = \sigma_S\left(\varepsilon_{\max} - \frac{\sigma_S}{E}\right) wF\left(\frac{dw}{da}\right) da \tag{25}$$

where the function F is defined as

$$F(n) = 2\left(\frac{(1+n)\sqrt{1+2n}}{n} - n\cot^{-1}\left(\frac{n}{\sqrt{1+2n}}\right) - \frac{(1+2n)^{3/2}}{n^2}\ln\left(\frac{1+2n}{1+n}\right)\right) \tag{26}$$

Therefore, the contribution of the process zone to toughness is

$$\Delta J_P = \frac{dU_P}{da} = \sigma_S\left(\varepsilon_{\max} - \frac{\sigma_S}{E}\right) wF\left(\frac{dw}{da}\right) \tag{27}$$

The size of the process zone can now be incorporated. Using Eq. (13):

$$\frac{dw}{da} \approx \frac{E}{4\sigma_S^2}\frac{dJ}{da} \tag{28}$$

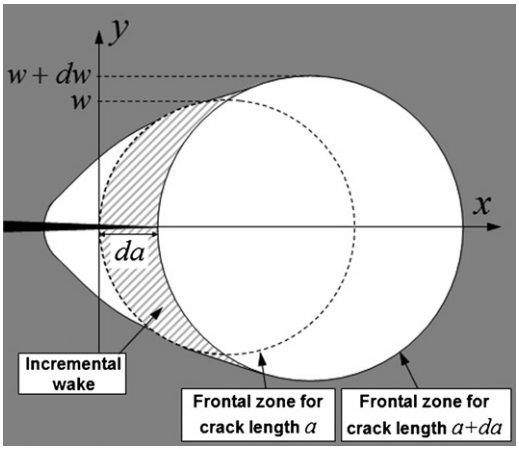

Fig. 7. Non-steady crack for the case where the width of the process zone increases with crack advance.

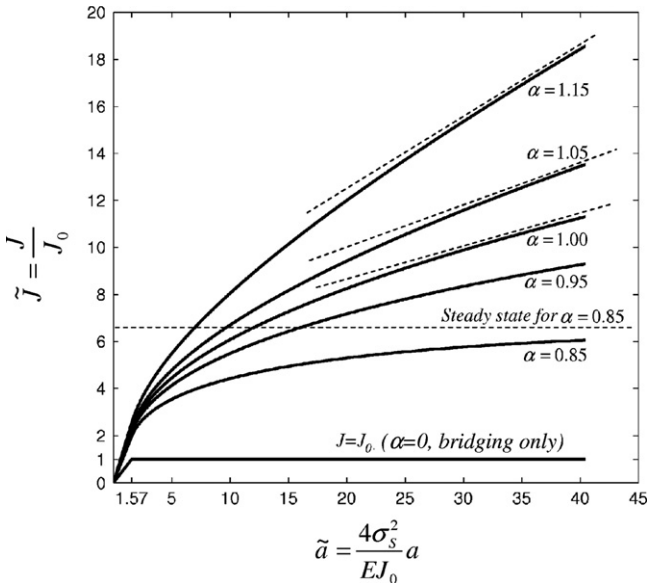

Fig. 8. Non-dimensional crack resistance curves for different values of the process zone parameter α.

Therefore, the total toughness can be written as

$$J = J_B + \Delta J_P = J_B + \alpha F\left(\frac{E}{4\sigma_S^2}\frac{dJ}{da}\right)J \tag{29}$$

where the transient bridging term J_B is provided by Eq. (23). Using Eq. (23) and defining a non-dimensional toughness $\tilde{J} = J/J_0$ and a non-dimensional crack advance $\tilde{a} = 4\sigma_S^2/EJ_0 a$, Eq. (29) becomes

$$\begin{cases} \tilde{J} = \frac{\frac{2}{\pi\tilde{a}}}{1-\alpha F\left(\frac{dJ}{da}\right)} & \text{for} \quad 0 \le \tilde{a} \le \frac{\pi}{2} \\ \tilde{J} = \frac{1}{1-\alpha F\left(\frac{dJ}{da}\right)} & \text{for} \quad \frac{\pi}{2} < \tilde{a} \end{cases} \tag{30}$$

Note that for a steady state process zone $d\tilde{J}/d\tilde{a} = 0$, $F(0)=1$, $J_B=J_0$ and Eq. (21) for steady state is recovered. This model is therefore consistent with the well established steady state solution. In order to solve Eq. (30), a numerical approach was used for different values of the process zone parameter α between 0 and 1.15, resulting in the non-dimensional crack resistance curves shown in Fig. 8. For all cases the toughness initially increases with crack advance, as the cohesive zone and inelastic wake develop. For cases where $\alpha < 1$, $\tilde{J}(\tilde{a})$ eventually reaches steady state, while for $\alpha \ge 1$ no steady state is reached and $\tilde{J}(\tilde{a})$ continuously increases towards an asymptotic branch of slope $1/F(1/\alpha)$. A rising crack-resistance curve has a profound impact on the reliability of the material. In effect, toughness increases as the crack advances, so that cracks emanating from defects within the material tend to be arrested and stabilized. A rising crack resistance curve is associated to damage tolerance in ceramics (Evans, 1990), and was also recently measured in a variety of hard biological materials such as bone (Ager et al., 2006), nacre (Barthelat and Espinosa, 2007), and dentin (Kruzic et al., 2003). The present model shows that increasing α results in an increase of toughness, and that large values of α lead to toughness which increases indefinitely with crack advance. This interesting phenomenon may be common in nature, since no steady state cracking could be achieved in nacre, bone or dentin. The toughness would then be only limited by how much volume of material is available to accommodate the increasing size of the process zone. The process zone parameter α may therefore be the most important parameter controlling toughness in staggered natural composites.

The validity of the model was also assessed by comparing its predictions with available experimental data for nacre (Rabiei et al., 2010) (Fig. 9). The experimental crack-resistance curves were obtained for red abalone using a four-point notched bending configuration (more details on the experimental setup and procedure can be found in Rabiei et al., 2010). The model prediction is presented in Fig. 9 for the range α=1.15–4 (as computed above for red abalone) which shows good agreement with the experiments. The predicted size and shape of the process zone were also compared to experimental observations (Rabiei et al., 2010) (Fig. 10). Again experiments and model show good agreement. Note that in the experiment the inelastic region was confined by weaker planes in the material called growth lines. Overall, the agreement of the model with the experiments is remarkable, which suggests that the model properly captures the fracture mechanics of staggered composites.

Finally, the predictions of the fracture model are displayed on material properties charts (Figs. 11 and 12). These charts were built based on the properties of nacre from red abalone (Rabiei et al., 2010) and of its constituents: mineral (Wegst

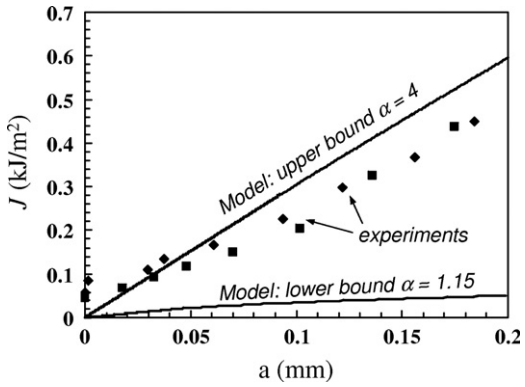

Fig. 9. Crack resistance curves obtained from the present model with two experimental curves from red abalone nacre (Rabiei et al., 2010).

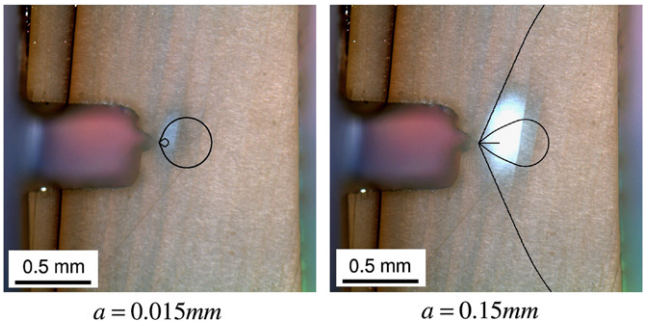

Fig. 10. Process zone for two crack advances. The experimental process zone is whiter than the surrounding material. The black lines represent the lower (α=1.15) and upper (α=4) process zone bounds from the present model.

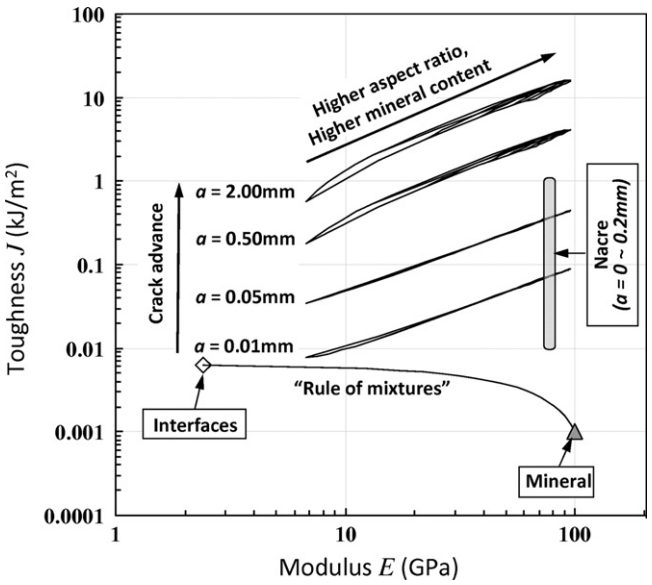

Fig. 11. Fracture toughness–modulus chart for red abalone nacre (Rabiei et al., 2010) and for its components (mineral (Wegst and Ashby 2004) and interfaces (Barthelat et al., 2007)). The predictions of the model for different crack advances are also shown. Note that the effects of mineral content and aspect ratio collapse into single lines.

and Ashby, 2004) and interfaces (Barthelat et al., 2007). The predictions of the model agree again well with existing experimental data. The tremendous amplification of toughness in nacre compared to its constituents and to the rule of mixtures (also shown in Fig. 10) is evident. In this regard toughness can be put in contrast with modulus and strength,

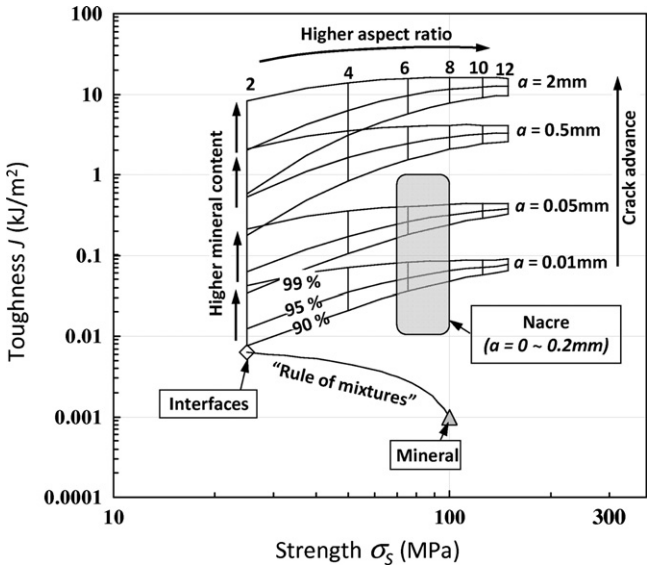

Fig. 12. Fracture toughness–strength chart for red abalone nacre (Rabiei et al., 2010) and for its components (mineral (Wegst and Ashby, 2004) and interfaces (Barthelat et al., 2007)). The predictions of the model for different crack advances are also shown.

which are bound by the modulus and strength of the constituents. A useful result in the context of biomimetics is that overall, large mineral contents and large aspect ratios lead to higher toughness. The model shows that staggered structures can achieve high modulus, high strength and high toughness simultaneously. This is remarkable considering the fact that in traditional engineering materials only one of these properties can be increased at a time at the expense of another (e.g. strengthening steel makes it more brittle).

4. Conclusions

The staggered structure is found in a variety of high-performance biological materials such as bone, nacre, mammalian teeth, and spider silk. This structure has emerged from natural evolution as an elegant solution to achieve useful combinations of stiffness, strength, and toughness. In line with existing analytical models for modulus and strength based on micromechanics, the present work provides a model for toughness, which for the first time, incorporates the concurrent micromechanics of bridging and process zone toughening. This analytical approach is relatively simple compared to numerical models based, for example, on cohesive elements. Numerical models for the fracture of staggered structures would be computationally expensive since both micromechanics at the microscale tablets and toughening at the millimeter size process zone would need to be included.

We found that the toughness of the interfaces is first amplified by inclusion pullout, and then further amplified by process zone toughening. For this reason both of these mechanisms are required for high overall toughness. The proposed model is in good agreement with experimental data from red abalone nacre.

The model also provides insights into microstructure–property relationships useful in the context of biomimetics. For example, increasing the mineral content or the aspect ratio of the inclusions leads to increased modulus, strength, and toughness. There are, however, design constraints: For example high aspect ratio may lead to premature fracture of the inclusion, a detrimental fracture mode that eliminates bridging and process zone. We found that the amount of toughness amplification (with respect to the interface toughness) is controlled by a "process zone parameter" α, a non-dimensional material property. Materials with high modulus, low strength and large strain at failure lead to high values for α, up to cases where process zone toughening is so intense that the crack does not reach steady state ($\alpha \geq 1$). This case is relevant for a tough material like nacre, and may be common in other staggered structures found in nature. It would be very interesting to duplicate these conditions in biomimetic staggered materials: an ever increasing toughness leads to steeper crack resistance curves, to more stable crack propagation and to increased material reliability and damage tolerance.

This model captures the micromechanics of staggered composites using continuum approaches and as such it cannot capture important mechanisms occurring at molecular scales (which are also critical to the overall performance of the material, Buehler and Yung, 2009; Buehler, 2007; Smith et al., 1999). This continuum approach can however complement atomistic models towards full multiscale descriptions of the deformation and failure in these sophisticated materials.

Finally, the fact that the staggered structure and its associated mechanisms can be found over several length scales in for example bone could have interesting implications in terms of overall performance. In particular, it would be interesting to explore the synergies of toughness amplifications provided by each length scale (Gao, 2006).

Despite significant recent efforts, duplicating the toughness of nacre in artificial materials remains a challenge (Munch et al., 2008). The fracture model presented here provides new insights that can prove invaluable in the development of bio-inspired, composite materials of superior toughness. In addition, this model may provide clues on the origin of bone toughness at the smallest length scales (Ritchie et al., 2009).

Acknowledgments

This work was supported by a Discovery Grant from the Natural Sciences and Engineering Research Council of Canada.

References

Ager, J.W., Balooch, G., Ritchie, R.O., 2006. Fracture, aging, and disease in bone. Journal of Materials Research 21 (8), 1878–1892.
Ballarini, R., et al., 2005. Biological structures mitigate catastrophic fracture through various strategies. International Journal of Fracture 135 (1–4), 187–197.
Barthelat, F., 2007. Biomimetics for next generation materials. Philosophical Transactions of the Royal Society A—Mathematical Physical and Engineering Sciences 365 (1861), 2907–2919.
Barthelat, F., 2010. Nacre from mollusk shells: a model for high-performance structural materials. Bioinspiration and Biomimetics 5 (3), 1–8.
Barthelat, F., et al., 2007. On the mechanics of mother-of-pearl: a key feature in the material hierarchical structure. Journal of the Mechanics and Physics of Solids 55 (2), 225–444.
Barthelat, F., Espinosa, H.D., 2007. An experimental investigation of deformation and fracture of nacre-mother of pearl. Experimental Mechanics 47 (3), 311–324.
Barthelat, F., Espinosa, H.D., 2007. The Deformation and Fracture of Nacre-mother of Pearl in SEM Annual Conference, Springfield, MA.
Buehler, M.J., Yung, Y.C., 2009. Deformation and failure of protein materials in physiologically extreme conditions and disease. Nature Materials 8 (3), 175–188.
Buehler, M.J., 2007. Molecular nanomechanics of nascent bone: fibrillar toughening by mineralization. Nanotechnology 18, 29.
Currey, J.D., 1977. Mechanical properties of mother of pearl in tension. Proceedings of the Royal Society of London 196(1125), 443–463.
Evans, A.G., et al., 1986. Mechanisms of toughening in rubber toughened polymers. Acta Metallurgica 34 (1), 79–87.
Evans, A.G., 1990. Perspective on the development of high-toughness ceramics. Journal of the American Ceramic Society 73 (2), 187–206.
Fantner, G.E., et al., 2005. Sacrificial bonds and hidden length dissipate energy as mineralized fibrils separate during bone fracture. Nature Materials 4 (8), 612–616.
Gao, H.J., 2006. Application of fracture mechanics concepts to hierarchical biomechanics of bone and bone-like materials. International Journal of Fracture 138 (1–4), 101–137.
Gao, H.J., et al., 2003. Materials become insensitive to flaws at nanoscale: lessons from nature. Proceedings of the National Academy of Sciences of the United States of America 100(10), 5597–5600.
Gupta, H.S., et al., 2006. Cooperative deformation of mineral and collagen in bone at the nanoscale. Proceedings of the National Academy of Sciences of the United States of America 103(47), 17741–17746.
Jackson, A.P., Vincent, J.F.V., Turner, R.M., 1988. The mechanical design of nacre. Proceedings of the Royal Society of London 234(1277), 415–440.
Jager, I., Fratzl, P., 2000. Mineralized collagen fibrils: a mechanical model with a staggered arrangement of mineral particles. Biophysical Journal 79 (4), 1737–1746.
Keten, S., et al., 2010. Nanoconfinement controls stiffness, strength and mechanical toughness of beta-sheet crystals in silk. Nature Materials 9(4), 359–367.
Kotha, S.P., Li, Y., Guzelsu, N., 2001. Micromechanical model of nacre tested in tension. Journal of Materials Science 36 (8), 2001–2007.
Kruzic, J., et al., 2003. Crack blunting, crack bridging and resistance-curve fracture mechanics in dentin: effect of hydration. Biomaterials 24 (28), 5209–5221.
Lawn, B.R., 1993. Fracture of Brittle Solids, Cambridge Solid State Science Series 2nd ed. Cambridge University Press, New York.
Launey, M.E., Ritchie, R.O., 2009. On the fracture toughness of advanced materials. Advanced Materials 21 (20), 2103–2110.
Mayer, G., 2005. Rigid biological systems as models for synthetic composites. Science 310 (5751), 1144–1147.
McMeeking, R.M., Evans, A.G., 1982. Mechanics of transformation-toughening in brittle materials. Journal of the American Ceramic Society 65 (5), 242–246.
Munch, E., et al., 2008. Tough, bio-inspired hybrid materials. Science 322 (5907), 1516–1520.
Ortiz, C., Boyce, M.C., 2008. Materials science—bioinspired structural materials. Science 319 (5866), 1053–1054.
Okumura, K., de Gennes, P.G., 2001. Why is nacre strong? Elastic theory and fracture mechanics for biocomposites with stratified structures. European Physical Journal E 4 (1), 121–127.
Peterlik, H., et al., 2006. From brittle to ductile fracture of bone. Nature Materials 5 (1), 52–55.
Rabiei, R., Bekah, S., Barthelat, F., 2010. Failure mode transition in nacre and bone-like materials. Acta Biomaterialia 6, 4081–4089.
Ritchie, R.O., Buehler, M.J., Hansma, P., 2009. Plasticity and toughness in bone. Physics Today 62 (6), 41–47.
Sarikaya, M., Aksay, I.A. (Eds.), 1995. Polymers and Complex Materials. AIP, Woodbury, NY.
Smith, B.L., et al., 1999. Molecular mechanistic origin of the toughness of natural adhesives, fibres and composites. Nature (London) 399 (6738), 761–763.
Song, F., Bai, Y.L., 2003. Effects of nanostructures on the fracture strength of the interfaces in nacre. Journal of Materials Research 18, 1741–1744.
Wang, R.Z., et al., 2001. Deformation mechanisms in nacre. Journal of Materials Research 16, 2485–2493.
Wegst, U.G.K., Ashby, M.F., 2004. The mechanical efficiency of natural materials. Philosophical Magazine 84 (21), 2167–2181.
Weiner, S., Wagner, H.D., 1998. The material bone: structure mechanical function relations. Annual Review of Materials Science 28, 271–298.